

# The Chip-Scale Atomic Clock – Low-Power Physics Package

R. Lutwak\*, J. Deng, and W. Riley  
Symmetricom - Technology Realization Center<sup>†</sup>

M. Varghese, J. Leblanc, G. Tepolt, and M. Mescher  
Charles Stark Draper Laboratory

D.K. Serkland, K.M. Geib, and G.M. Peake  
Sandia National Laboratories<sup>††</sup>

Abstract

*We have undertaken a development effort to produce a prototype chip-scale atomic clock (CSAC). The design goals include short-term stability,  $\sigma_y(\tau) < 6 \times 10^{-10} \tau^{-1/2}$ , with a total power consumption of less than 30 mW and overall device volume  $< 1 \text{ cm}^3$ . The stringent power requirement dominates the physics package architecture, necessarily dictating a small ( $< 1 \text{ mm}^3$ ) volume gaseous atomic ensemble interrogated by a low-power semiconductor laser. At PTTI 2002 and PTTI 2003, we reported on laboratory experiments which underlie the fundamental architecture of our CSAC, based on interrogation of the cesium D1 transition by the technique of coherent population trapping (CPT).*

*In the past year, the development effort has shifted from fundamental research and feasibility investigation to engineering and prototype development. In this paper, we report on the design of a rugged and compact physics package that is expected to exceed the ultimate performance and power requirements of the CSAC.*

## INTRODUCTION

We are developing a chip-scale atomic clock (CSAC) with the goal of producing a  $1 \text{ cm}^3$  device that can provide a stability of  $1 \times 10^{-11}$  over 1 hour while consuming only 30 mW. While the stability goals are modest, equivalent to  $\sigma_y(\tau=1) = 6 \times 10^{-10}$ , the power and size goals are quite ambitious, each more than two orders of magnitude smaller than existing technology.

---

\* E-mail: [RLutwak@Symmetricom.com](mailto:RLutwak@Symmetricom.com)

<sup>†</sup> 34 Tozer Rd., Beverly, MA 01915

<sup>††</sup> Sandia is a multiprogram laboratory operated by Sandia Corporation, a Lockheed Martin Company, for the United States Department of Energy's National Nuclear Security Administration under contract DE-AC04-94AL85000.

Conventional gas cell atomic clocks employ a gaseous atomic sample, contained in a resonant microwave cavity which is tuned to the ground state hyperfine frequency,  $\nu_{\text{HF}}$ . An RF lamp assembly illuminates the resonance cell and optically pumps the atomic ensemble into one of the two hyperfine levels. Redistribution of the atomic states is driven by resonant microwaves, applied to the cavity and servoed to  $\nu_{\text{HF}}$  so as to re-equilibrate the populations. This conventional architecture, termed “optical-microwave double resonance interrogation,” necessarily dictates the use of rubidium for the atomic species, due to the fortunate coincidence of near overlap of the optical transitions from the  $|5S_{1/2}, F = 2\rangle$  ground state of  $\text{Rb}^{87}$  with those of the  $|5S_{1/2}, F = 3\rangle$  ground state of  $\text{Rb}^{85}$ . This is the architecture employed in all commercially available gas cell frequency standards. The evolution of this technology has led to its miniaturization and power reduction to the point that commercial standards are now available with size  $<125\text{cm}^3$  and power consumption  $<10$  Watts [1]. Nonetheless, the size and power consumption remain far too high for portable battery-powered applications. The principal limitations of the conventional technology in this regard are power consumption of the lamp assembly, which typically requires  $>1$  W to produce sufficient optical power, and the size of the RF cavity, whose dimensions are determined by the centimeter-scale wavelength of the  $\nu_{\text{HF}}$ . The ambitious goals of the CSAC require a new approach to the fundamental physics of the atomic interrogation.

In prior PTTI proceedings[2-3], we have reported on laboratory experiments which explored alternative approaches to interrogation of the atomic resonance and considered their performance tradeoffs for the CSAC program. In [2], we compared conventional interrogation, utilizing a low-power Vertical Cavity Surface Emitting Laser (VCSEL) in place of the conventional lamp, with the approach of Coherent Population Trapping (CPT). In the CPT approach, the interrogating RF is applied, at  $\nu_{\text{HF}}/2$ , directly to the bias of the VCSEL, thereby producing a balanced pair of first-order sidebands separated by  $\nu_{\text{HF}}$ . In that study, it was determined that the CPT approach could provide adequate stability to meet the CSAC stability goals, in smaller size and at lower power than the conventional approach. In [3], a custom VCSEL was developed to compare the expected performance utilizing either the cesium D1 or D2 optical transitions, at  $\lambda=894$  nm and  $\lambda=852$  nm respectively. It was shown that the D1 transition delivers 5X superior performance to D2, with no additional cost of power or size. Based on this experimental effort, we have proceeded with development of the CSAC, with an architecture based on CPT interrogation of atomic cesium, utilizing a VCSEL laser, tuned to the cesium D1 optical transition at  $\lambda=894$  nm and directly modulated at  $\nu_{\text{HF}}/2=4.6$  GHz.

In this paper, we report on the development of a novel physics package design, which implements this fundamental architecture, while minimizing its size and power consumption. We describe the geometry as well as the construction and test of components which will comprise the completed physics package.

## FOLDED OPTICS GEOMETRY

For design purposes, we have divided our 30 mW power budget into three parts, allowing 10 mW each for the physics package, control circuits, and RF subsystem. In this section, we describe a novel interrogation geometry, termed “Folded Optics,” which allows the implementation of a physics package which meets the CSAC stability goals within its 10 mW power budget.

The power consumption of the physics package is dominated by the requirement to heat the sample of cesium atoms to  $75^\circ\text{C}$  in order to produce a gaseous sample of sufficient density to support the statistically limited signal/noise requirements of the CSAC. Naturally, the necessary power is dictated by the thermal losses from the physics package to the ambient environment. In our case, the key thermal loss mechanisms include gaseous convection, thermal radiation, and conduction through the gaseous

environment, the cell support structure, and the electrical leads. Gaseous convection and conduction can be effectively eliminated by enclosing the heated physics package in a vacuum package. Conduction through the electrical leads is inescapable, but can be minimized by reducing the cross-section of the leads and maximizing the length, insofar as possible without sacrificing reliability. The remaining components of heat loss, thermal radiation and conduction through the support structure, are both minimized by making the physics package as small as possible. In the case of thermal radiation, the heat loss is proportional to the radiating area and, in the case of the support structure, minimizing the mass of the physics package permits reducing the cross-section of its supports. For these reasons, it is essential to make the physics package as small as possible, within the performance constraints of the CSAC project.

For the purposes of discussion, **Figure 1** shows the physics package components usually employed for laboratory interrogation by the method of CPT. Separate ovens are used for stabilizing the VCSEL in order to tune it to the cesium wavelength and for the resonance

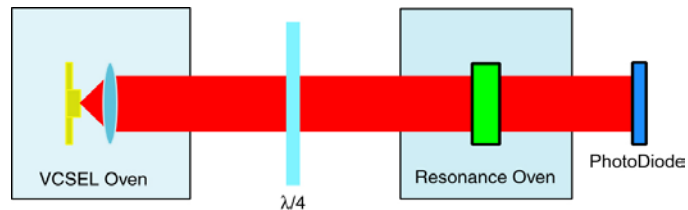


**Figure 1: Traditional CPT interrogation geometry**

oven in order to maintain the optimum cesium vapor density. The divergent output from the VCSEL is allowed to propagate until its diameter matches the aperture of the resonance cell, at which location a lens of suitable focal length collimates the beam. A quarter-wave polarization retarder ( $\lambda/4$ ) converts the linearly polarized laser beam into circular polarization which passes through the atomic vapor. The intensity of the transmitted beam is monitored by a photodetector.

There are several limitations of the traditional CPT geometry that must be overcome in order to minimize its size and power consumption. It is relatively straightforward to minimize the component spacing between the  $\lambda/4$ -plate, the resonance cell, and the photodiode. In order to reduce the size and power consumption further, the two separate ovens must be combined into a single temperature-controlled region in order to avoid the size, complexity, and electronic overhead of maintaining two separate temperature-controlled regions. This requires that the VCSEL be designed to tune to the cesium wavelength at the same temperature as the optimum temperature of the resonance cell. Initially, this is a yield issue and requires selecting devices from the VCSEL wafer of appropriate wavelength. Ultimately, this will become an issue of process control in order to develop wafers of uniform optimum wavelength devices. The remaining path length, which cannot be simply removed, is the necessary divergence distance between the VCSEL aperture and the collimating lens. This distance is determined by the fundamental divergence properties of the VCSEL and the required beam diameter to efficiently illuminate the resonance cell. A typical VCSEL laser, with half-angle divergence of  $12^\circ$ , requires 2.5 mm distance between the VCSEL aperture and collimating lens to produce a 1 mm diameter beam. In the CSAC, this collimation distance nearly doubles the size, and radiative heat loss, of the physics package.

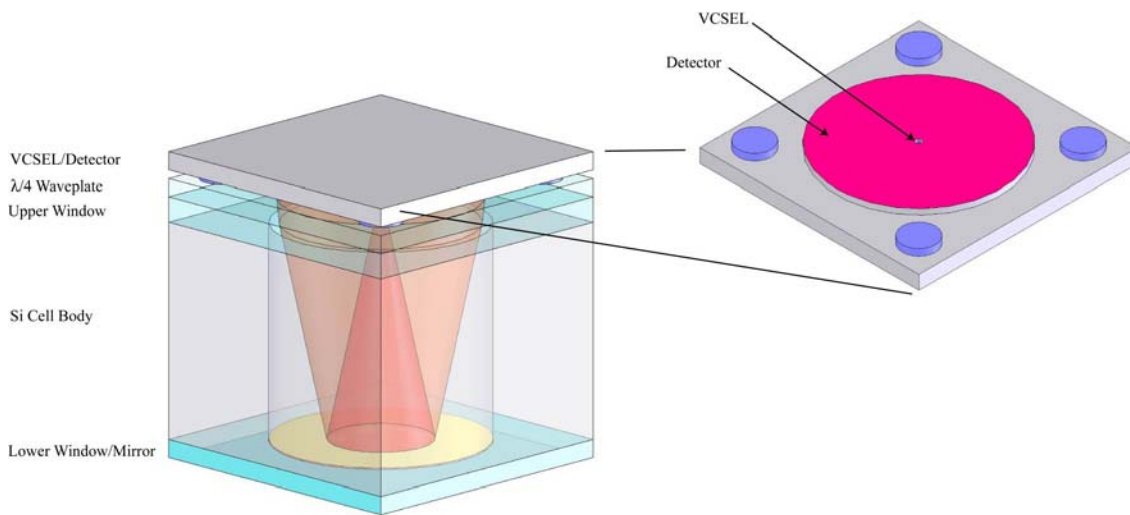


**Figure 2: Folded-optics geometry**

**Figure 2**, above, illustrates our folded-optics geometry. The topmost component includes the VCSEL, located at its center, as well as the 1.5 mm diameter photodetector, which surrounds the VCSEL. The divergent laser beam, shown in red, emerges from the VCSEL and continues to diverge as it passes through the cesium vapor cell, retro-reflects from a mirrored surface, and passes through the cell a second time before returning to the photodetector. The feature of folded optics which enables its compact design is that the laser beam is not collimated. By matching the dimensions of the resonance cell to the natural divergence of the VCSEL output beam, folded optics permits efficient illumination of the atomic volume without the additional length required for collimation.

**PHYSICS PACKAGE OVERVIEW**

The CSAC physics package has been designed to implement the folded optics architecture described above in order to minimize size and power consumption. Because of its small size and relatively high degree of complexity, modern semi-conductor and batch processing techniques are employed wherever possible to minimize handling of the delicate components and reduce the cost of assembly.

The key components of the physics package are identified in **Figure 3** and are described in greater detail in subsequent sections. The heart of the CSAC physics package is the cesium resonance cell, which is fabricated of silicon, loaded with cesium metal and inert buffer gas, and sealed with Pyrex windows, one of which is copper-plated to provide the retro-reflection for the folded optics interrogation.

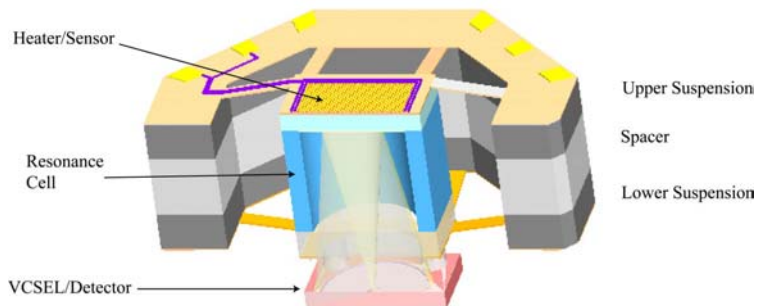


**Figure 3: Cutaway view of CSAC physics package**

The cesium cell is supported by a strained polyimide support structure which provides minimal thermal conductivity to the rigidly-mounted silicon frame. The heater and temperature sensor are patterned onto the upper polyimide suspension and the leads are patterned onto the legs of the suspension. The lower suspension includes leads and bond pads for the VCSEL/Detector component, which is subsequently installed onto the suspended cell assembly. A prototype physics package assembly is shown in **Figure 4**.

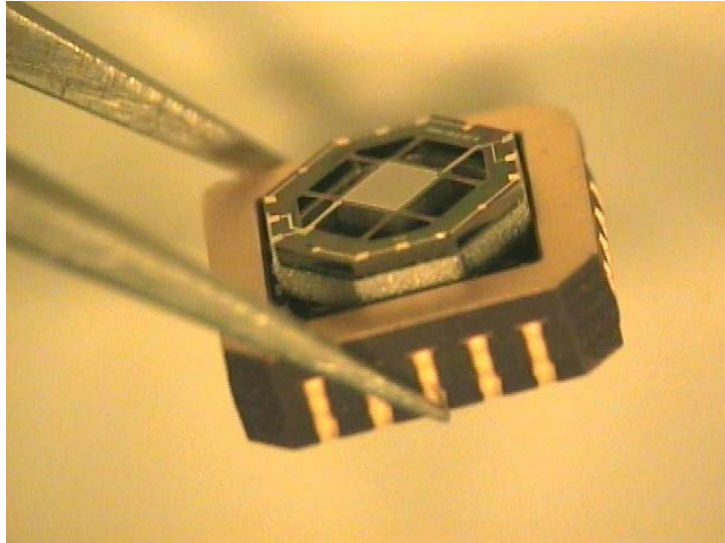


**Figure 4: Prototype physics package**

### **CESIUM RESONANCE CELL**

With low cost and high volume in mind, MEMS batch fabrication processes have been developed to produce cesium resonance cells. These cells consist of a cavity defined in silicon, with Pyrex top and bottom windows anodically bonded to the silicon cell body (see **Figure 5(a)**). The top Pyrex window is transparent for laser interrogation of the cell and a copper reflector is patterned onto the bottom Pyrex window to support the folded optics configuration.

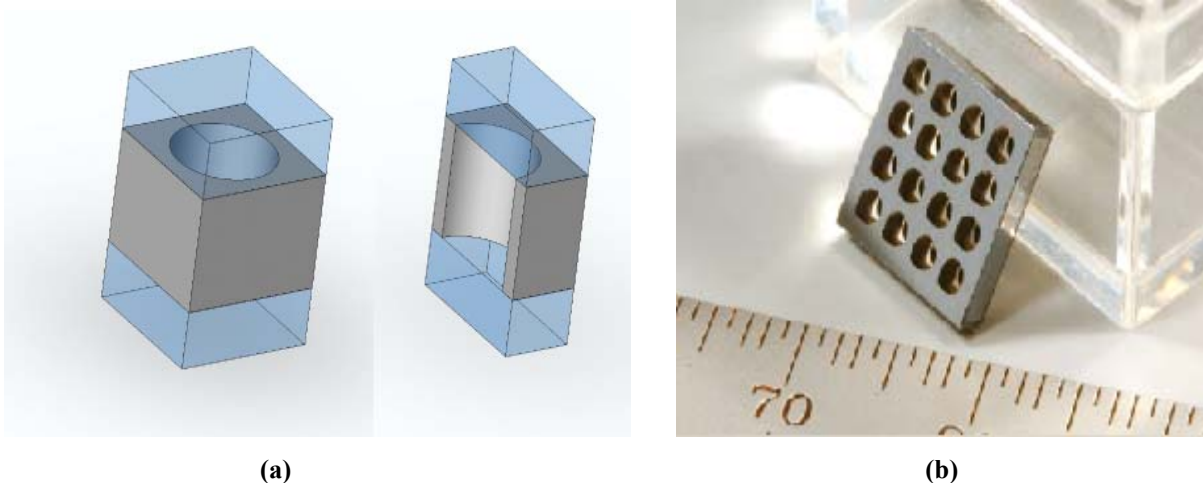


**Figure 5: (a) Single Cesium resonance cell with silicon cavity (gray) and Pyrex top and bottom caps (blue). (b) 1 cm<sup>2</sup> tablet containing sixteen cells.**

**Figure 5(a)**, above, shows schematics of the cesium resonance cell. On the right, the photograph in **Figure 5(b)** shows an experimental 1 cm<sup>2</sup> “tablet” of 16 cells. In production quantities, as many as 500 cells could be fabricated on a single four-inch diameter wafer. The cells are fabricated as follows. Starting with a clean 250 μm thick Pyrex wafer, the mirrors are created by depositing 3000 Å of copper sandwiched between two 400 Å titanium layers and photolithographically patterned by a liftoff technique. The array of cavities is micromachined through a 1.5 mm silicon wafer using the technique of deep reactive ion etching (DRIE). The lower window, with patterned mirrors, is anodically bonded to the silicon cavity array. The array of open cavities is then transferred to an anaerobic glovebox wherein cesium can be loaded into the cells without oxidation, following the technique pioneered by NIST [4]. A small volume (1-10 nl) of cesium is dispensed into the cells prior to batch sealing using a small volume pipette. Such a technique may be automated and scaled to dispense quickly into thousands of cells, similar to techniques for spotting of microarrays in biological research. After loading with cesium, the open array of cavities is moved into a hermetically-sealed bonding apparatus which is then evacuated and backfilled with the measured pressure of temperature-compensated buffer gas mixture. Performing the final anodic bond of the transparent top window to the cell array requires careful timing and process control because the bonding process requires raising the cell assembly to 350 °C. At this elevated temperature care must be taken to control the final buffer gas pressure and to prevent the cesium vapor from interfering with the bonding process. Finally, the sealed array of cesium resonance cells is removed from the bonder and diced into individual 2 mm x 2 mm cells.

Essential performance parameters of the cesium resonance cells are summarized in **Table 1**.

Traditionally, the resonance cells for rubidium frequency standards have been fabricated of Pyrex or other alkali-resistant glasses. The frequency aging properties of this type of cell are poorly understood though generally attributed to changes in the buffer gas composition due to prolonged interaction with the cell walls. The use of DRIE silicon for the cell body may introduce risk into the CSAC project because the frequency aging of this material system is unknown.

|                  |  |
|------------------|--|
| Cavity depth     | 1.5 mm   |
| Cavity diameter  | 1.5 mm   |
| Cavity Volume    | 2650 nl  |
| Outer dimensions | 2 mm x 2 mm x 2.125 mm                         |
| Buffer Gas       | Temperature-compensated N <sub>2</sub> /Ar mix |

**Table 1: Cesium resonance cell specifications**

In order to investigate cell aging effects in the anodically-bonded glass-silicon-glass CSAC resonance cells, as well as to verify compliant clock stability with cells of this size and composition, several prototype cells were tested in our laboratory CPT apparatus, at our design temperature of 75 °C, in the traditional topology of **Figure 1**.

**Figure 6** shows a 3-day frequency record of a prototype anodically-bonded glass-silicon-glass cell installed in our laboratory CSAC testbed frequency standard. The linear fit indicates a drift of  $d\bar{y}/dt = +3 \times 10^{-11}/\text{day}$ . It is clear, though, from **Figure 6**, that the long-term frequency variations are dominated by factors other than linear drift, notably temperature variations in the laboratory. This drift rate is exceptionally good, particularly for a relatively “young” cell when compared with the early drift rates of conventional blown glass cells. While this result is encouraging, it reflects a relatively short data set and further drift-rate measurements will need to be made once integrated temperature-stabilized physics packages become available. The Allan deviation of this frequency record, shown in **Figure 7** indicates short-term stability of  $\sigma_y(\tau) \approx 4 \times 10^{-11} \tau^{-1/2}$

from  $\tau=1$ -100 seconds, more than an order-of-magnitude better than the DARPA specification for the CSAC. The deviation from the ideal  $\tau^{-1/2}$  behavior at long  $\tau$  is primarily due to temperature sensitivity of the VCSEL output power in the laboratory environment. We can thus conclude that the anodically-bonded glass-silicon-glass cell, as specified by **Table 1**, produces adequate signal level, contrast, and linewidth to support the goals of the CSAC program.

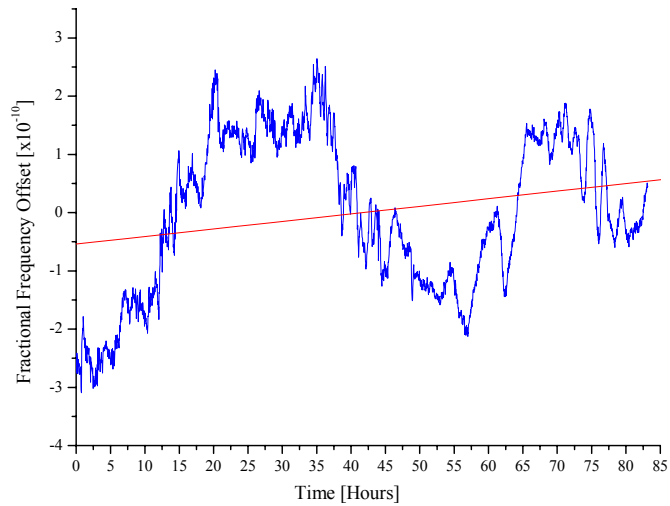


**Figure 6: 3-day Frequency record of prototype cell**

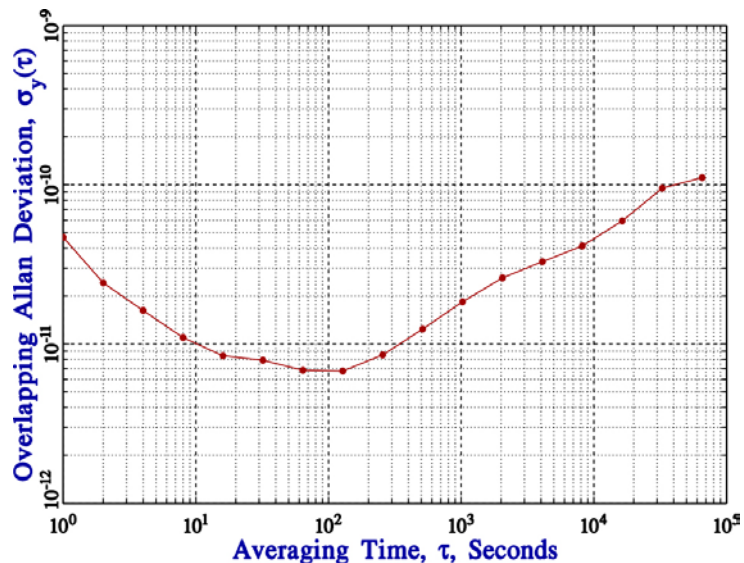


**Figure 7: Allan deviation of data set of Figure 6**

## CELL SUSPENSION

The purpose of the cell suspension system is to minimize conductive thermal losses from the heated resonance cell while providing the necessary mechanical support for a rugged device.

Our design goals for the suspension system are shown in **Table 2**. The degree of thermal insulation required to meet the power budget significantly limits the choice of materials and the beam dimensions of the suspension system. The

| Specification      | Value               |
|--------------------|---------------------|
| Power              | <10 mW              |
| Volume             | < 1 cm <sup>3</sup> |
| Resonant frequency | >2 kHz              |
| Shock load         | >1500 g             |

**Table 2: Cell suspension engineering goals**

suspension system must, however, be stiff and rugged. Moreover, as with all aspects of the CSAC design, we seek to develop a construction technique which lends itself to low-cost high-volume batch manufacturing. This combination of constraints has led to the development of a novel suspension system employing strained polyimide support tethers. Polyimide has extremely low thermal conductivity (less than 0.2 W/m °C) and a high strain yield (typical 3%). In order to make the device robust against large accelerations, the suspension beams are angled so that they resist motion in a tension rather than bending mode. Two sets of suspension systems are used, one on top and one on the bottom of the resonance cell. The lower suspension, shown in **Figure 8(a)** below, has leads and bond pads for flip-chip attachment of the VCSEL/Detector assembly. The upper suspension, including the cell heater and temperature sensor is shown in **Figure 8(b)**.

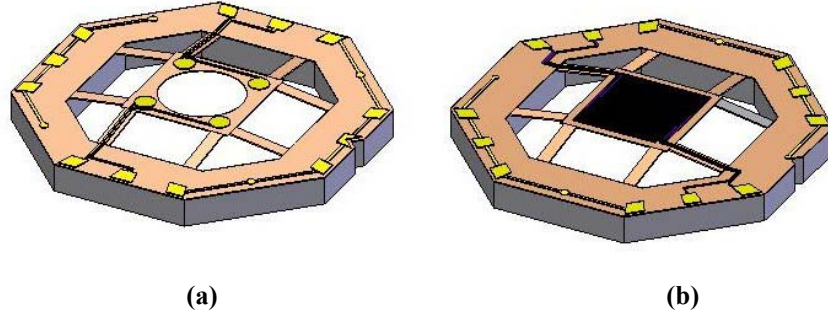


**Figure 8: Lower (a) and upper (b) suspension assemblies**

The suspension components are fabricated using “planar” fabrication techniques. The lower suspension, shown in **Figure 8(a)**, is created by spin-coating 5  $\mu\text{m}$ 's of photodefinable polyimide onto a 500  $\mu\text{m}$  silicon wafer. The suspension pattern is developed and cured. The leads are composed of 0.4  $\mu\text{m}$  of Au and 0.4  $\mu\text{m}$  of Pt, with a thin Ti adhesion layer. The bond pads are 0.5  $\mu\text{m}$  gold. The leads and bond pads for the VCSEL/detector assembly are deposited and patterned by magnetron sputtering and liftoff. Finally, the suspension is released by a through-wafer backside ICP silicon etch. The upper suspension is fabricated similarly. The heater and temperature sensor traces and leads are composed of 0.25  $\mu\text{m}$  of Pt with Ti for adhesion.

The angle of the suspension beams is established during the assembly of the resonance cell with the suspension components. This is achieved in a controlled fashion by adjusting the height of the vapor cell to slightly exceed the spacing between the outward facing faces of the frame portions of the suspension components. This assembly procedure pretensions the suspension members, with a larger angle

generating a larger pretension and overall suspension stiffness, limited by the acceptable design strain in the suspension beams.

The calculated frequency of the first mechanical resonance and strain in the tethers are plotted as a function of tether angle in **Figure 9**. The choice of polyimide as the tether material is critical because it has a high strain limit (i.e. can be stretched a large amount relative to other low-thermal-conductivity materials such as silicon nitride or oxide). Thus mechanically robust designs are enabled by a significant tether angle, but this is readily constructed using a planar suspension component fabrication process only if the tether material has a high strain limit, as polyimide does.

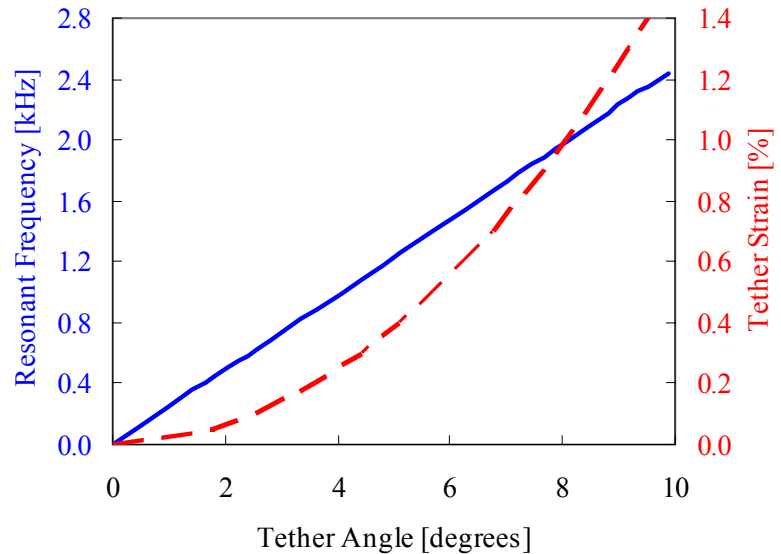


**Figure 9: Cell resonant frequency and tether strain**

The cell temperature is maintained through integrated

single-element resistive platinum heating and temperature-sensing elements, which are patterned onto the polyimide suspension. The heater resistance (400Ω) is distributed around the periphery of the cell only, which, because the end-cap of the vapor cell is a poor thermal conductor and the cell is hollow, provides heat only in areas where it can be most uniformly distributed, resulting in a more uniform temperature than if the heating resistance was distributed uniformly over the surface of the cell window. The temperature sensor (10kΩ) is distributed over the cell window to provide an accurate average temperature measurement of the vapor cell. In order to reduce magnetic fields due to current flowing in the heater and temperature sensor, both are patterned as bifilar pairs such that current flowing through one segment of the resistor is balanced by the opposing current of another segment in close proximity.

In a vacuum enclosure, the key contributions to thermal loss from the suspended cell assembly are conduction, through the tethers and patterned electrical leads, and radiation from the cell body. We use a model equation to describe the heater power P required to maintain a cell in vacuum at a temperature  $T_{\text{cell}}$  given by:

$$P = \frac{(T_{\text{cell}} - T_{\text{ambient}})}{R_{\text{cond}}} + A_{\text{cell}} \cdot \varepsilon \cdot \sigma \cdot (T_{\text{cell}}^4 - T_{\text{ambient}}^4)$$

where  $R_{\text{cond}}$  is the thermal conduction resistance of the suspension structure and electrical leads, which is calculated from the suspension geometry and known materials properties.

A complete model for radiation loss from the cell would incorporate the effects of the shape factors and emissivities, as well as multiple reflections from the various radiating surfaces. The equation above captures the temperature dependence by lumping these coefficients into a single emissivity term  $\epsilon$  associated with a cell area  $A_{\text{cell}}$ .  $T_{\text{cell}}$  and  $T_{\text{ambient}}$  are the equilibrium temperatures of the heated cell and ambient environment, respectively, and  $\sigma$  is the Stefan-Boltzman constant. To verify the thermal performance of the cell suspension system, a prototype physics package was mounted in vacuum and the cell temperature was measured as a function of heater power. The data is shown in

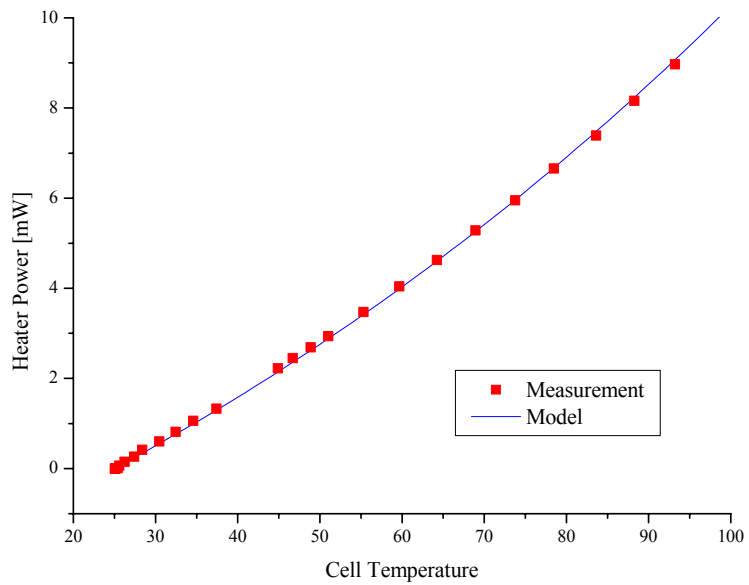


**Figure 10: Experimental verification of thermal design**

**Figure 10** along with the theoretical model with  $R_{\text{cond}}=75^{\circ}\text{C}/\text{mW}$  and  $\epsilon=0.57$ .

### VCSEL/PHOTODETECTOR ASSEMBLY

A custom integrated VCSEL (vertical-cavity surface-emitting laser) / RCPD (resonant-cavity photodiode) chip at 894 nm was designed and fabricated at Sandia National Laboratories in order to enable the folded-optics approach. A photograph of the 2 mm x 2 mm chip is shown in **Figure 11(a)**. The VCSEL is located at the center of the chip and is shown emitting light in the close-up view of **Figure 11(b)**. Surrounding the VCSEL is a 1.5 mm diameter RCPD. Electrical connections to the VCSEL and RCPD are provided by the four round bond pads located at the corners of the chip.

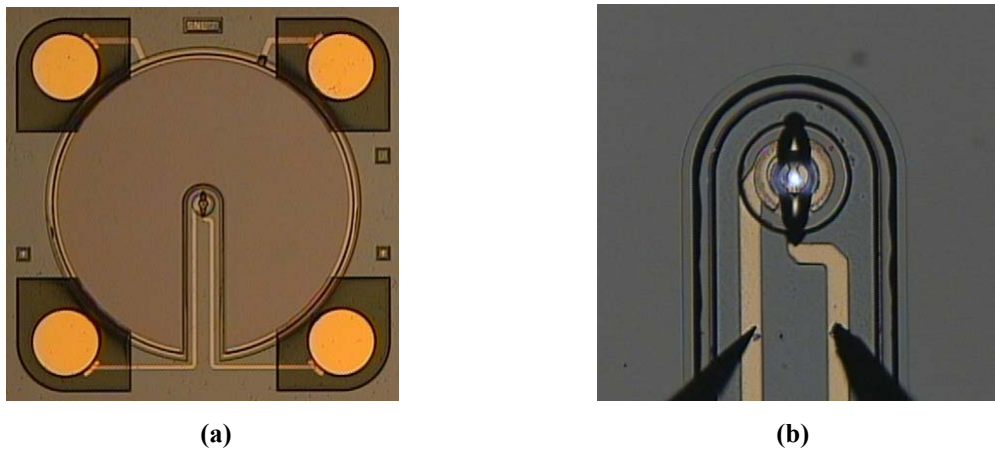


**Figure 11: (a) Photograph of VCSEL/RCPD chip and (b) close-up of the VCSEL operating above threshold**

A cross-sectional view of the VCSEL and RCPD structures is shown in **Figure 12**. The epitaxial semiconductor layers of the 894 nm VCSELs are grown on a semi-insulating GaAs substrate to minimize parasitic capacitances. The bottom distributed Bragg reflector (DBR) is designed as a high reflector, containing 36 pairs of n-doped quarter-wave high-index  $\text{Al}_{0.16}\text{Ga}_{0.84}\text{As}$  and low-index  $\text{Al}_{0.92}\text{Ga}_{0.08}\text{As}$  layers. The active region contains 5 undoped (intrinsic)  $\text{In}_{0.07}\text{Ga}_{0.93}\text{As}$  quantum wells (QWs) to provide optical gain near 890 nm. A quarter-wave layer of p-doped  $\text{Al}_{0.98}\text{Ga}_{0.02}\text{As}$  immediately above the active region is selectively oxidized to form a circular oxide aperture that confines current to the center of the device. The oxide aperture diameter is kept below 4 microns so that the VCSEL emits predominantly in the fundamental transverse mode. The top DBR is designed as an output coupling mirror, containing 21 pairs of p-doped quarter-wave low-index and high-index layers. The output power and voltage versus current data for a 3 micron aperture VCSEL are shown in **Figure 13**. Notice that the threshold is only 0.3 mA at 1.54 V, so that less than 1 mW of DC electrical power is required to operate the VCSEL.

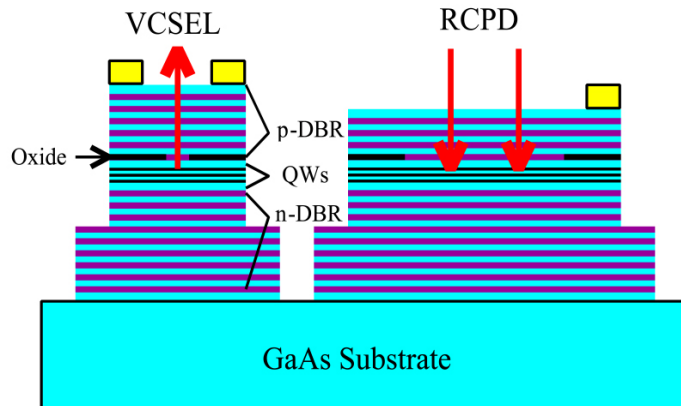


**Figure 12: Schematic cross-sectional view of VCSEL and RCPD structures (not to scale)**

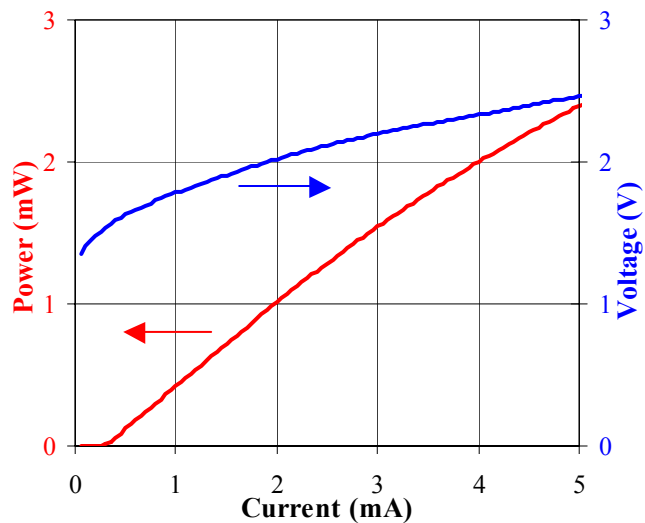


**Figure 13: VCSEL power and voltage vs. current**

The VCSEL has been optimized for single longitudinal and transverse mode operation in a single linear polarization. The optical emission spectrum of the VCSEL at a drive current of 1.0 mA is shown in **Figure 14**. The spectrum shows that the higher order transverse modes are suppressed by more than 30 dB relative to the fundamental transverse mode.

The resonant-cavity photodiode (RCPD) is fabricated using the same epitaxial material as the VCSEL, but part of the top DBR is etched away to improve the optical impedance match by reducing the top mirror reflectivity from 99.77% to 97.18%. The responsivity versus wavelength of a test RCPD device is shown in **Figure 15**. The half-maximum-response bandwidth of the RCPD shown in **Figure 15** is 2.8 nm. The emission spectrum (on a linear scale) of a single-mode VCSEL located near the RCPD is superimposed on the responsivity plot to show the relative spectral alignment of the VCSEL and RCPD. Since the VCSEL and RCPD share the same epitaxial material, their nominal resonance wavelengths coincide and will track each other with changes in the ambient temperature. However, as suggested in **Figure 15**, the VCSEL resonance wavelength is slightly blue shifted due the transverse optical confinement of the small oxide aperture[5]. Note that

the emission from a VCSEL located at the center of an RCPD would likely be somewhat more blue-shifted than that shown in **Figure 15**. However, driving more current into the VCSEL will locally heat the laser and red-shift its emission into better alignment with the RCPD resonance.

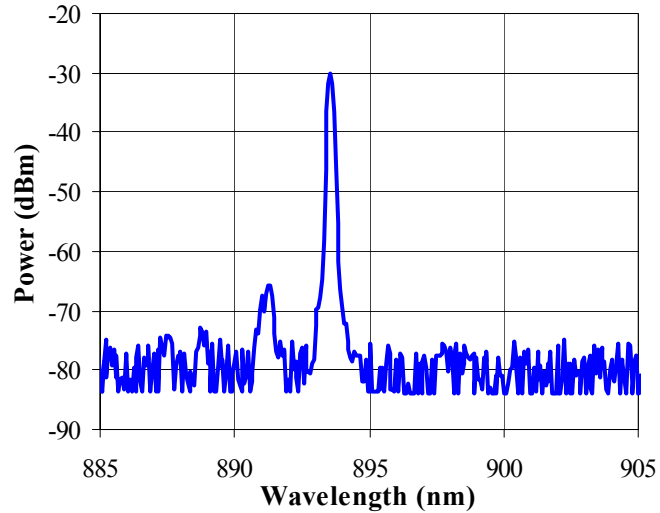


**Figure 14: VCSEL emission spectrum**

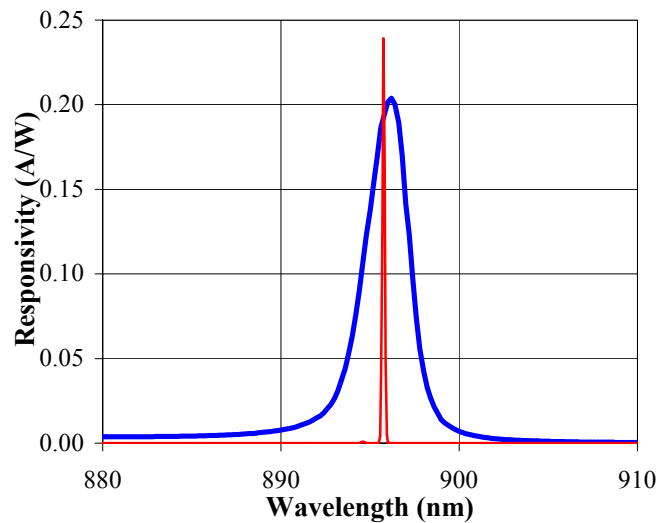


**Figure 15: RCPD Responsivity versus wavelength (blue). VCSEL emission spectrum (red).**

## PHYSICS PACKAGE ASSEMBLY AND PACKAGING

The physics package is assembled as shown in **Figure 16**. Excluding the VCSEL/RCPD assembly, the components are stacked up as shown in **Figure 16** and mounted with low-vapor pressure epoxy, the polyimide tethers are angled by clamping to the frame spacer until the epoxy sets. Following assembly of the cell and suspension, the VCSEL/Detector assembly is bump-bonded to the lower suspension bond pads with 0.018" indium-based solder. The contacts from the package to the VCSEL/Detector are made by directly soldering the bond pads on the polyimide suspension to the mating pads on the inside of the LCC. The heater/sensor connection, from the upper suspension are made with gold wire bonds.

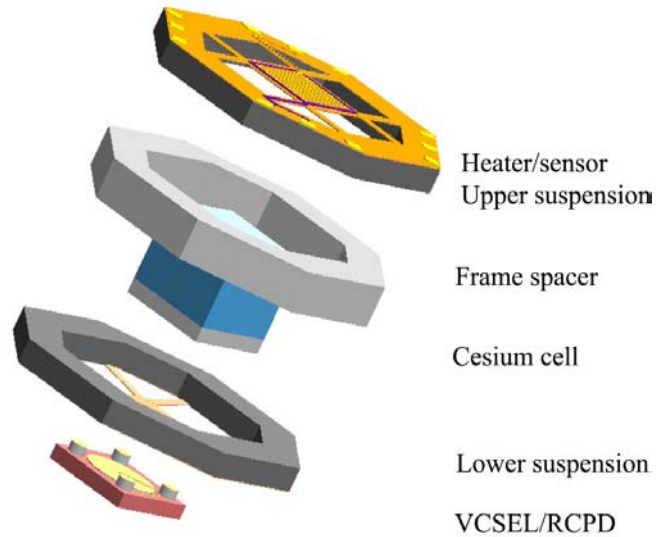
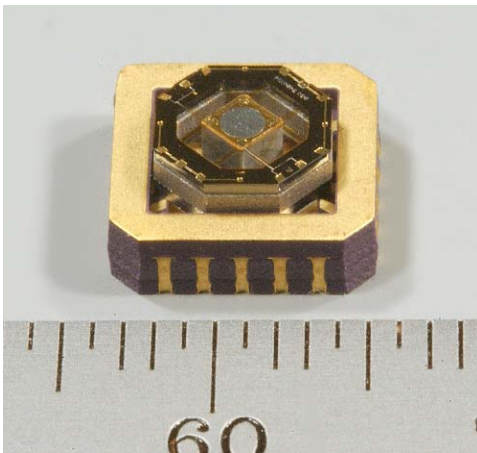
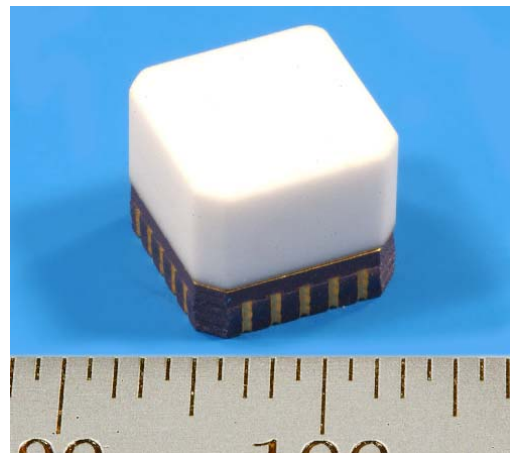


**Figure 16: Exploded view of physics package components**



(a)



(b)

**Figure 17: Physics package in LCC (a) with lid removed and (b) with lid installed**

The LCC package is sealed in a vacuum environment. The top lid is fabricated from  $\text{Al}_2\text{O}_3$  ceramic and is lined with a temperature-activated titanium-based getter. Within the vacuum sealing apparatus, the getter is activated and the lid is installed and brazed onto the LCC.

## ACKNOWLEDGEMENTS

The authors wish to thank Mike Garvey, of the Symmetricom TRC, and John McElroy of Draper Laboratory, for supporting and directing this effort. We are also thankful for the technical and theoretical support provided by Don Emmons and Peter Vlitras of the Symmetricom TRC. We thank V. M. Montano and A. T. Ongstad for assistance in the fabrication of the VCSEL/RCPD chips and T. W. Hargett for assistance in the epitaxial semiconductor growth. This work is supported by the Defense Advanced Research Projects Agency, Contract # NBCHC020050.

## REFERENCES

- 
- [1] see, for example, <http://www.symmetricom.com/media/pdf/documents/ds-x72.pdf>
- [2] R. Lutwak, et. al., “The Chip-Scale Atomic Clock – Coherent Population Trapping vs. Conventional Interrogation”, *Proceedings of the 34<sup>th</sup> Annual Precise Time and Time Interval (PTTI) Systems and Applications Meeting*, December 3-5, 2002, Reston, VA, pp. 539-550.
- [3] R. Lutwak, et. al., “The Chip-Scale Atomic Clock – Recent Development Progress”, *Proceedings of the 35<sup>th</sup> Annual Precise Time and Time Interval (PTTI) Systems and Applications Meeting*, December 2-4, 2003, San Diego, CA, pp. 467-478.
- [4] L-A. Liew, et. al. “Microfabricated alkali atom vapor cells,” *Applied Physics Letters*, **84**, p. 2694 (2004).
- [5] D. K. Serkland, G. R. Hadley, K. D. Choquette, K. M. Geib, and A. A. Allerman, “Modal frequencies of vertical-cavity lasers determined by an effective-index model,” *Appl. Phys. Lett.*, **77**, 22-4 (2000).